Food Chemistry 502 (2026) 147681

Contents lists available at ScienceDirect

Food Chemistry

journal homepage: www.elsevier.com/locate/foodchem

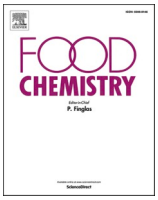

Development of a hydrophobic chain linker MIL-53(Al) as a sorbent in pipette tip-μSPE method for the determination of bisphenols in food packaging

Helan Zeyad Sami [a], Lazgin Abdi Jameel [b], Soleiman Moinfar [a,c,*]

[a] Chemical Analysis Research Center, Scientific Research Center, University of Zakho, Zakho, Iraq
[b] Chemistry Department, College of Science, University of Zakho, Zakho, Iraq
[c] Department of Basic Sciences, College of Pharmacy, Nawroz University, Duhok, Iraq

ARTICLE INFO

Keywords:
Dual-linker mil-53(Al)
Pipette tip-μSPE
Food analysis
Bisphenols
HPLC-PDA

ABSTRACT

Pristine aluminum-based metal-organic framework (MIL-53(Al)) as a sorbent shows limited affinity toward bisphenols due to the lack of hydrophobicity in its framework. To overcome this limitation, a dual-linker MIL-53 (Al) with a hydrophobic carbon chain linker was synthesized for the first time and integrated into a pipette tip-micro solid-phase extraction (PT-μSPE) method for bisphenol determination. The parameters affecting the extraction process were optimized by implementing a response surface methodology (RSM) model using central composite design (CCD). Brunauer-Emmett-Teller analysis confirmed substantial increases in pore volume and pore width for the dual-linker MIL-53(Al) (0.74 cm^3/g; 5.3 nm) compared with pristine MIL-53(Al) (0.17 cm^3/g; 1.22 nm). This modification boosted the extraction efficiency of dual-linker MIL-53(Al) for bisphenols determination, resulting in low detection limits (0.01–0.1 μg/L), wide linearity (0.033–200.0 μg/L), high enrichment factors (up to 209), and good precision (RSD $\leq$ 7.0 %) in tea, disposable cups and containers, instant noodles, PET water bottles.

1. Introduction

Bisphenols (BPs) are a group of synthetic compounds containing two hydroxyphenyl functional groups, which are essential in the manufacturing process of plastics, notably epoxy resins and polycarbonates, and other polymeric materials. Among them, bisphenol A (BPA) also known as 2,2-bis(4-hydroxyphenyl)propane, is the most extensively manufactured and researched among the numerous bisphenol compounds, followed by structurally related analogues such as bisphenol F (BPF) which is referred to as 4,4′-(dihydroxydiphenylmethane), and bisphenol AF (BP AF), known as 4,4′-(hexafluoroisopropylidene) diphenol, which are increasingly used as BPA substitutes (Michałowicz, 2014; Vandenberg et al., 2012). BPA and its substitutes are widely used in commercial products, present in food-contact materials, including container linings, plastic packaging, medical devices, thermal paper, and household items (Catron et al., 2019; Lehmler et al., 2018). Numerous monitoring studies have confirmed the widespread migration of BPA and its analogues into food and beverages, with concentrations up to tens of ng/g depending on food type and processing (Kaykhaii et al., 2020; Liao & Kannan, 2013; Noonan et al., 2011). One study conducted in the United States detected BPA in 63.0 out of 105.0 food samples, corresponding to a detection rate of 60.0 %. The samples included both fresh foods and those packaged in cans or plastic containers, with BPA concentrations ranging from below the limit of quantification (<0.20 ng/g wet weight) to 65.0 ng/g. (Schecter et al., 2010). Due to concerns over endocrine-disrupting effects, many authorities have restricted BPA usage in infant products and food packaging, resulting in the increased industrial application of BPF, BPAF, and related substitutes (D. Chen et al., 2016; Jala et al., 2022). With increasing consumer demand for food safety and the ongoing need to maintain product quality, packaging materials have become widely utilized in food preservation applications (M. J. Khan et al., 2024). The growing complexity of packaged foods and the extensive global use of polymeric packaging materials have intensified concerns regarding chemical migration into food that compromises both safety and public health (Gupta et al., 2024). Smart packaging, such as colorimetric sensors (Escher et al., 2023), freshness indicators (Shao et al., 2021), and antimicrobial films (OuYang et al., 2025), has emerged as a promising

* Corresponding author at: Chemical Analysis Research Center, Scientific Research Center, University of Zakho, Zakho, Iraq.
E-mail address: soleiman_moinfar@yahoo.com (S. Moinfar).

https://doi.org/10.1016/j.foodchem.2025.147681
Received 24 July 2025; Received in revised form 6 December 2025; Accepted 20 December 2025
Available online 25 December 2025

technology for improving food quality monitoring and reducing contamination risks (S. Khan et al., 2025). Nevertheless, smart packaging materials are cost-effective and may contain polymer additives or contaminants that can migrate under certain storage, food composition, and temperature conditions (Palanisamy et al., 2025). Therefore, effective analytical detection of bisphenols remains essential, independent of packaging innovations. Accurate quantification of bisphenols in foods is hindered by matrix interferences, low analyte levels (often <1 ng/g), and the need for highly sensitive instrumentation, including HPLC and LC-MS/MS methodologies (Kamal et al., 2025; Martín-Gómez et al., 2024). Therefore, to mitigate these issues, there is a pressing need to devise a straightforward, efficient, and sensitive sample preparation method that can substantially diminish matrix effects and concentrate trace analytes to ensure accurate determinations, such as solid phase extraction (SPE) (Ding et al., 2024). SPE has limitations, including complex procedures, high solvent and sorbent usage, and inconsistent reproducibility (Meng et al., 2022; Peñalver et al., 2021). For this reason, miniaturized extraction techniques have been developed to address these issues to improve sensitivity, reduce solvent consumption, and simplify experimental workflow. Among these sample treatment methods, the following methods can be mentioned: dispersive solid-phase extraction (DSPE)(Ahmed et al., 2025), magnetic solid-phase extraction (MSPE)(H. L. Jiang et al., 2021a; S. Li et al., 2022), solid phase microextraction (SPME) (Zhu et al., 2024), syringe-filter packed solid-phase extraction (SF-SPE) (Moinfar, Khodayari, Sami, et al., 2022a), miniaturized stir bar sorptive dispersive microextraction (mSBSD-ME) (López-Juan et al., 2024), and pipette-tip micro solid-phase extraction (PT-μSPE) (Silva Maciel et al., 2024). PT-μSPE uses only a small amount of sorbent, typically a few milligrams, packed between two small plugs of cotton inside a pipette tip. This configuration allows rapid adsorption and desorption, while requiring very little elution solvent. This miniaturized technique provides both economic and practical benefits, establishing it as a promising approach for modern analytical applications (Wang et al., 2024).

The efficiency of the solid phase extraction methods greatly depend on the sorbent material, which must provide selective interactions with bisphenols through hydrophobic forces, hydrogen bonding, π–π stacking, or electrostatic interactions(Wang et al., 2023). Consequently, sorbents capable of establishing these specific interaction forces with BPs are prioritized in the selection process. Nowadays, a range of porous materials, including porous organic polymers (Gandomkar et al., 2025), covalent organic frameworks (COFs) (Song et al., 2025), and metal-organic frameworks (MOFs) (M. Chen et al., 2025), have been utilized to extract and enrich target compounds. MOFs are highly ordered 3D crystalline structures formed by coordinate connections between metal ions and organic linkers. Their large surface area, functional diversity, high porosity, and tunable surface chemistry make them particularly effective adsorbents for extracting a wide range of chemicals. This versatility has spurred interest in their interactions with other pollutants, including co-exposure scenarios involving bisphenol compounds, highlighting MOFs' growing role in various fields, notably in food analysis (Lv et al., 2025; N. Zhang et al., 2025).

Although MOFs, particularly MIL-53(Al), have previously been used for bisphenol extraction, their performance can be constrained by limited pore environments and inadequate hydrophobic interactions with the analytes (Zahmatkesh Anbarani & Bonyadi, 2025; G. Zhang, Wo, Sun, Xiao, et al., 2021). In this study, to enhance the efficiency of MIL-53(Al), a dual-linker version of the material was synthesized and employed as an adsorbent in pipette-tip micro-solid phase extraction (PT-μSPE). For the first time, lauric acid was incorporated as a secondary linker, selected for its long aliphatic chain that can improve pore tunability and strengthen hydrophobic interactions with the target compounds. Modified MIL-53(Al) with different lauric acid/terephthalic acid ratios (15 and 30 % *w*/w) was synthesized and evaluated. The extraction efficiency of the different synthesized dual-linker MIL-53(Al) was compared with the pristine MIL-53(Al) under the same conditions. Key extraction parameters were systematically optimized using Design-Expert software. The resulting dual-linker MOFs were applied as sorbents in PT-μSPE for the preconcentration and determination of bisphenols in plastic containers and food samples, followed by quantification using high-performance liquid chromatography with photodiode array detection (HPLC-PDA). Overall, this strategy aims to develop a more efficient sorbent for trace bisphenols analysis in complex food matrices. This work demonstrates a strong potential for routine application in food safety monitoring.

2. Materials and methods

2.1. Chemicals

Analytical standards of Bisphenol A supplied from (SigmaAldrich - Taiwan). Bisphenol AF, Bisphenol F, and Luaric acid ($CH_3(CH_2)_{10}COOH$) were purchased from (SigmaAldrich - USA). Terephthalic acid (C_6H_4–1,4-$(CO_2H)_2$) (BDC) was supplied from (Bio-ChemoPharma - France). Sodium hydroxide (NaOH) and aluminum nitrate nonahydrate ($Al(NO_3)_3.9H_2O$) were acquired from (Carl Ruth - Spain). *N*, *N*-Dimethylformamide, was supplied from (Carlo-Erba - France). Acetonitrile (99.9 %) and methanol (99.9 %) were purchased from (Merck- Darmstadt, Germany), and hydrochloric acid (HCl) was provided from (Scharlau-Spain).

Suitable amounts of bisphenols were prepared monthly in methanol to generate a 400.0 mg/L stock solution and subsequently stored at a temperature of 4 °C. Before analysis, fresh working solutions in distilled water were generated through the precise dilution of the aforementioned standard solutions. All reagents, standards, and solvents are of analytical and synthetic grade.

2.2. Instrumentation

The extracted bisphenols were separated and quantified using HPLC from Flexar-PerkinElmer (USA) equipped with Luna 5u column C18 (250 × 4.6 mm, 5 μm particle size) from Phenomenex (USA) coupled to a photodiode array detector from Flexar-PerkinElmer (USA). The separation method utilized was gradient elution with ultrapure water (A) and acetonitrile (B). The separation was under the following HPLC conditions: The mobile phase flow rate was 1.0 mL/min, and 30 °C was set for column oven temperature. The wavelength of UV detection was 230 nm, and the injection volume was 35.0 μL. The gradient elution was as follows: initial condition 40 % B; 0–2.0 mins, 40 % to 85 % B; in 8.0 mins, 85 % to 30 % B; in 3.0 mins, then returning to the original conditions and equilibrating the column. The XRD (X-ray diffraction) patterns were acquired via a diffractometer (X-Pro, Philips, The Netherlands) with Cu-Ka radiation (l = 1.5418 A) in the angular area (2y) of 5–501.

The thermal gravimetric analysis (TGA) was obtained using (STA PT-1000 thermal analyzer (Linseis, Germany). FTIR spectra were recorded using a PerkinElmer Spectrum RXI spectrometer (USA). The Brunauer–Emmett–Teller (BET) was performed using a pore size and surface area distribution analyzer (Belsorp mini II analyzer, Japan) by nitrogen adsorption at 77 K in the range of $0.0001 \leq p/p_{\circ} \leq 0.9918$. For the surface morphology analysis, the LEO 1430VP (Germany) scanning electron microscopy (SEM) was utilized at 15.0 kV. The pH adjustments were done using (Eutech- pH 510) with the electrode of Adwa from Romania. For pumping the sample solution, a (205 U- Watson Marlow) peristaltic pump was used. The synthesis and drying steps were obtained in a LIKANG (China) electric oven. The JOANLAB hotplate stirrer was operated for stirring and heating purposes.

2.3. Synthesis of pristine MIL-53(Al), and dual-linkers MIL-53(Al)-BDC/LA

The frameworks of MIL-53(Al) and dual-linkers, MIL-53(Al)-BDC/LA

(85:15) and (70:30), were synthesized via a solvothermal process as illustrated in Fig. 1 (a). A mixture of 2 mmol of aluminum nitrate nonahydrate (0.75 g) and 1 mmol of benzene-1,4-dicarboxylic acid (0.166 g) in a 1:0.5 mol ratio was prepared in 50.0 mL of DMF. The mixture was ultrasonically homogenized for 30.0 min and then transferred to a 100 mL Teflon reactor in a stainless-steel autoclave. The autoclave capsule was heated in an oven at 120 °C for 48 h based on the previously reported MIL-53(Al) synthesis protocol (Majumder et al., 2020). For the synthesis of MIL-53(Al)-BDC/LA (85,15), a mixture of 2 mmol of aluminum nitrate nonahydrate (0.75 g), 0.85 mmol of BDC (0.14 g), and 0.15 mmol of lauric acid (0.03 g) was incorporated in 50.0 mL of DMF. For the synthesis of MIL-53(Al)-BDC/LA (70,30), a mixture of 2.0 mmol of aluminum nitrate nonahydrate (0.75 g), 0.7 mmol of BDC (0.116 g), and 0.3 mmol of lauric acid (0.06 g) was incorporated in 50.0 mL of DMF. Then homogenized mixtures were heated separately for 48 h at 120 °C in an autoclave. After the reaction, the products were recovered by centrifugation at 4000 rpm for 10 min, and then were stirred overnight in DMF to remove unreacted linkers. The materials were subsequently refluxed for 12 h, with methanol to eliminate residual DMF from the MOF pores, and dried at 80 °C in an electric oven for 24 h.

2.4. Preparation of the pipette tip

A 20.0 mg portion of each metal–organic framework (MOF) was accurately weighed and packed inside a 1.0 mL pipette tip. The sorbent was sandwiched between two small plugs of cotton, with one cotton plug placed at the narrow end of the pipette tip to prevent particle loss, and the second plug added on top to secure the packing material in place. After assembling the mini-column, 1.0 mL of deionized water was gently passed through the tip using a syringe. This conditioning step ensured that the MOF particles were properly compacted, uniformly wetted, and tightly fixed between the two cotton plugs, as illustrated in Fig. 1(a).

2.5. Procedure

The pH of both the spiked and unspiked food samples and the plastic containers' content was initially adjusted to 6.75 via 0.1 mol/L NaOH and 0.1 mol/L HCl solutions. Subsequently, 38.0 mL of each sample was processed through a peristaltic pump at a 2.0 mL/min flow rate and directed into a pipette tip containing the MOF sorbent, as shown in Fig. 1 (b). Later, the bisphenols captured by the sorbent were eluted using 150.0 µL of a mixture containing (60 % methanol and 40 % acetonitrile) as the desorption solvent. Finally, 35.0 µL of the desorbed solution was injected into an HPLC system.

2.6. Samples pre-treatment

For the preparation of food and packaging samples for BPA, BPF, and BPAF analysis, hot water was added to tea leaves in disposable cups and allowed to stand for a particular period. The resulting infusion was then filtered to remove suspended solids. Afterwards, the pH of the tea filtrate was adjusted to 6.75, and collected in two separate containers, each with 38.0 mL. Finally, the two aliquots were spiked with bisphenol standard solutions to obtain final concentrations of 30.0 and 100.0 µg/L, respectively. Also, hot water was added separately to the instant noodles' container, disposable containers, and cups. Each item was allowed to stand for 30.0 min to promote the leaching of bisphenols under typical consumer-use conditions. For bottled water, a sealed PET bottle was placed in a water bath at 45.0 °C for 30.0 min to simulate mild thermal exposure prior to consumption. After treatment, 38 mL of each sample was collected for analysis. The pH of all samples was adjusted to 6.75 to ensure consistency across matrices. For spiking experiments, 30.0 µg/L and 100.0 µg/L of the bisphenol standard solution were added to selected samples to evaluate method recovery and matrix effects.

2.7. Calculations of enrichment factor and relative recovery

The enrichment factor for each bisphenol was calculated using the following equation:

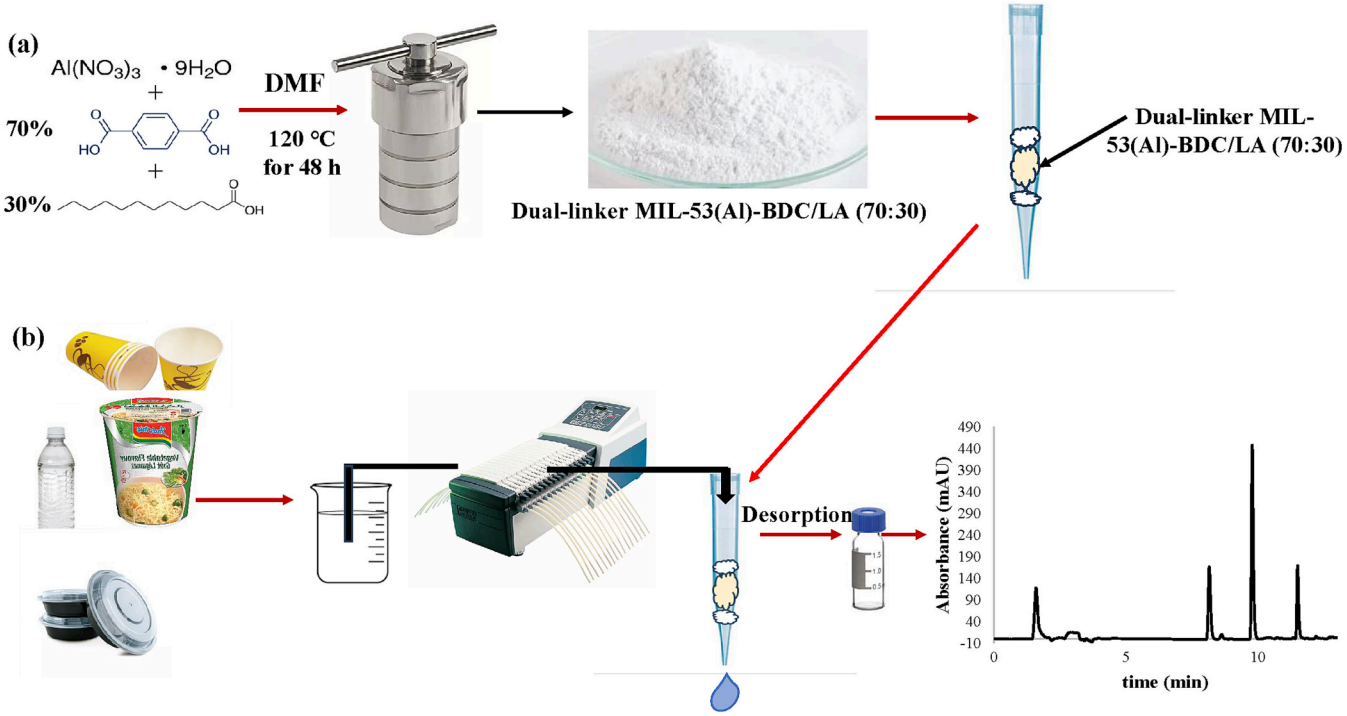

Fig. 1. An illustration scheme of (a) the synthesis of dual-linker MIL-53(Al)-BDC/LA (70,30) MOF and its placement in a pipette tip, (b) analysis of BPs in various food samples and packaging by PT-µSPE-HPLC-PDA.

$$EF = \frac{C_e}{C_{in}} \quad (1)$$

The enrichment factor (EF) is defined as the ratio of the analyte concentration in the extractant phase (C_e) to its initial concentration in the aqueous phase (C_{in}).

On the other hand, the relative recovery (RR) was calculated using the following equation:

$$RR\% = \frac{C_{spiked} - C_{nuspiked}}{C_{added}} \times 100 \quad (2)$$

In this equation, C_{spiked}, $C_{unspiked}$, and C_{added} represent the concentration of BPs after adding a standard solution to the samples, the original concentration of BPs in real samples, and the concentration of standard solutions added to the samples (Moinfar et al., 2021).

2.8. Central composite design for bisphenol extraction optimization

The optimization of factors affecting extraction was evaluated using dual-linker MIL-53(Al)-BDC/LA (70 %:30 %) as the sorbent material in a pipette tip for the PT-μSPE method. A central composite design (CCD) was applied as a response surface methodology to optimize the extraction of bisphenol compounds: BPF, BPA, and BPAF from food samples and plastic containers. Four factors were investigated: pH (3.5–10), sample volume (10–45 mL), desorption solvent volume (100–345 μL), and desorption solvent type (methanol, acetonitrile-methanol mixture, and acetonitrile). Design-Expert 13.0.5 software was used to perform 54 experimental runs that were conducted in randomized order to account for potential variability and interaction effects. The design used a reduced cubic model without blocks. The target responses were the peak areas (signal intensities) of BPF, BPA, and BPAF, as quantified via chromatographic analysis. The statistical modeling and optimization were performed using ANOVA to evaluate the significance of model terms and to determine optimal conditions for maximum extraction efficiency.

3. Results and discussion

3.1. Characterization

3.1.1. XRD analysis

X-ray diffraction (XRD) analysis was carried out to assess the crystallographic features and phase purity of pristine and dual-linker MIL-53(Al) samples, as shown in the Fig. 2(a). The diffraction patterns were recorded in the 2θ range of 5° to 80° using Cu Kα radiation. The diffraction pattern of MIL-53(Al) in Fig. 2a (a) shows characteristic peaks at approximately 2θ = 9.8°, 13.1°, 16.6°, 18.8°, and 22.4°, which can be indexed to the (110), (200), (211), (220), and (310) crystallographic planes, respectively, which correspond well to the reported planes of the MIL-53(Al) orthorhombic structure (Skans et al., 2025a). These reflections indicate the presence of the open-pore phase typically observed under ambient conditions, confirming successful formation of the pristine framework. Fig. 2a shows the XRD pattern of dual-linker MIL-53(Al)-BDC/LA (85:15) that exhibits slightly broader and less intense peaks compared to pristine MIL-53(Al), particularly at 2θ = 9.8°, 16.6°, and 18.8°, indicating that the framework preserves its original structure, yet undergoes subtle lattice distortion. This attenuation can be related to the incorporation of long-chain aliphatic lauric acid into the framework. In contrast, the pattern for the dual-linker MIL-53(Al)-BDC/LA (70:30) in Fig. 2a, more pronounced changes are observed, with peaks detected at 2θ ≈ 9.8°, 13.1°, 16.6°, and 18.8°, though with noticeably higher intensity, especially at the low-angle region. The sharp and intense peak at ~9.8° suggests a more ordered crystal structure, likely due to the dominance of terephthalic acid in maintaining the framework integrity (Pezhhanfar et al., 2022a). The slight shift or narrowing of peaks may be attributed to minor lattice distortions and expansion of the framework lattice from increased LA inclusion. These results are in agreement with literature reports on mixed-ligand metal-organic frameworks, where bulky or flexible ligands can distort or disrupt framework periodicity (Carrington et al., 2019; Ha et al., 2017; Pallach et al., 2021).

3.1.2. Evaluation of FT-IR spectra

Fourier-transform infrared (FT-IR) spectroscopy was employed to investigate the structural integrity and ligand incorporation within the pristine MIL-53(Al) framework and its dual-linker derivatives synthesized with varying ratios of lauric acid and terephthalic acid, as seen in Fig. S1. For pristine MIL-53(Al), a broad band was observed at 3502–3750 cm^{-1}, attributed to the O—H stretching vibration from bridging hydroxyl groups and adsorbed water. The asymmetric stretching of the carboxylate group (–COO^-) appeared at 1625 cm^{-1}, and a peak at 1423 cm^{-1} corresponded to the symmetric carboxylate stretching, confirming coordination of terephthalic acid to Al (III) centers. Vibrations at 1298 cm^{-1} and 1256 cm^{-1} were assigned to C—O

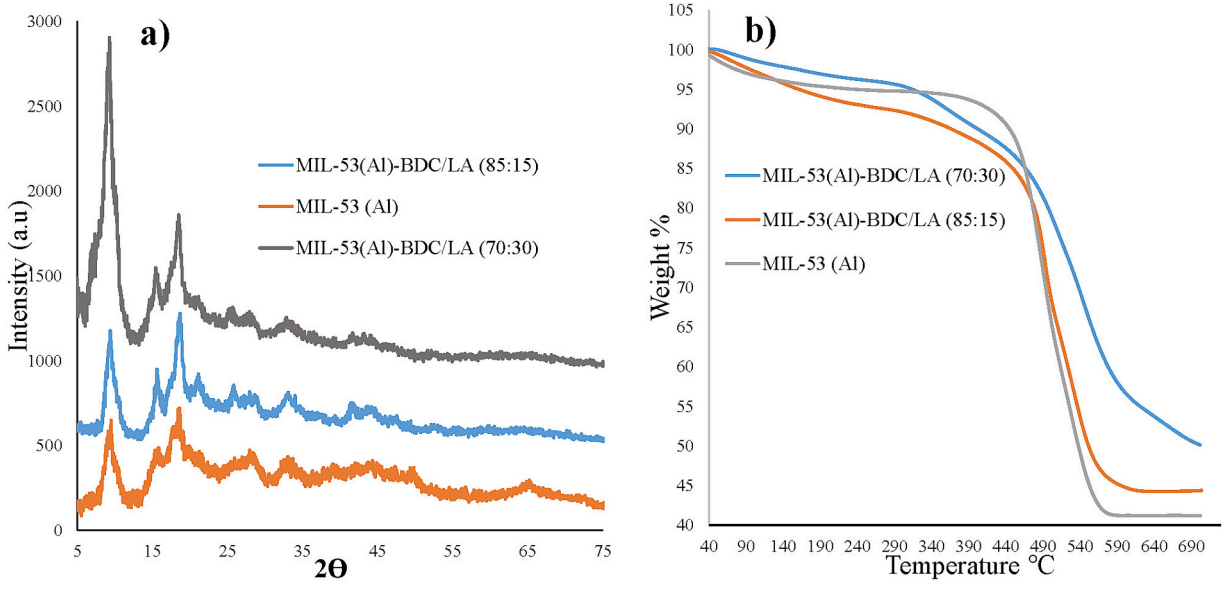

Fig. 2. (a) XRD patterns, and (b) TGA curves of MIL-53(Al), dual-linker MIL-53(Al)-BDC/LA (85,15), and dual-linker MIL-53(Al)-BDC/LA (70,30).

stretching and in-plane bending of aromatic rings, while peaks at 1138, 1095, and 1065 cm^{-1} were linked to C—C stretching within the aromatic backbone. The bands at 1025 and 990 cm^{-1} indicated C—H out-of-plane bending, and the peaks at 757, 592, and 518 cm^{-1} were associated with Al—O bond vibrations in the framework structure (Katugampalage et al., 2021; Pezhhanfar et al., 2022b). As for the dual-linker MIL-53(Al)-BDC/LA (85:15), the FT-IR spectrum revealed a broad O—H stretching band at 3447 cm^{-1}, with additional features in the 2959–2870 cm^{-1} region representing C—H stretching vibrations of the lauric acid's aliphatic chains. The carboxylate asymmetric and symmetric stretching bands were located at 1672 cm^{-1}, 1654 cm^{-1}, and 1452–1423 cm^{-1}, respectively, indicating successful coordination of both ligands. Aromatic C═C stretches were seen at 1614, 1542, and 1510 cm^{-1}, showing retention of the aromatic structure from terephthalic acid. The presence of aliphatic components was further supported by bands at 1326, 1299, and 1257 cm^{-1} (C—O and CH_2 deformations), and the C—C stretching and C—H wagging modes were visible in the 1094 to 996 cm^{-1} region (J. Jiang et al., 2018). The framework-related vibrations, including Al—O stretches, appeared prominently at 784, 758, 736, 726, and 596 cm^{-1}, with additional lattice vibrations at 481.94 cm^{-1}. In the case of dual-linker MIL-53(Al)-BDC/LA (70:30), the FT-IR spectrum showed a combination of both aromatic and aliphatic signatures. The O—H stretch remained broad in the 3400–3500 cm^{-1} range (not explicitly given in the current dataset but typically observed), while asymmetric and symmetric carboxylate stretches were observed around 1650–1450 cm^{-1}, confirming the mixed-ligand coordination. The C—H stretching and bending vibrations were around 2950–2870 cm^{-1} associated with Lauric acid. Aromatic skeletal and C—O stretching vibrations were present in the 1300–1000 cm^{-1} region, and Al—O related bands persisted below 800 cm^{-1}, indicating that the framework integrity was maintained. These assignments align well with previously reported spectra for MIL-53(Al) (Pezhhanfar et al., 2022c), and the ligand-modified analogs incorporate the long-chain carboxylic acids like lauric acid, introduce additional aliphatic stretching and bending features, while retaining the core coordination vibrations of the MOF structure.

3.1.3. TGA analysis

The thermal behavior of MIL-53(Al) and its dual-linker analogs containing lauric acid was assessed by applying TGA and recorded over a temperature range of 20 to 700 °C at a heating rate of 10 °C/min under an air atmosphere, as displayed in Fig. 2b. All three samples exhibit an initial weight loss below 150 °C of around 5 %, attributed to the release of physically adsorbed water and solvent residues. The MIL-53(Al) showed a major weight loss of around 50 % between 430 and 570 °C, corresponding to the decomposition of the organic BDC linker, which is characteristic of the thermal breakdown of the MOF framework (Rehman et al., 2025). On the contrary, the dual-linker samples (85:15) and (70:30) displayed an additional intermediate decomposition stage between 300 and 450 °C, consistent with the thermal degradation of lauric acid (Vennapusa et al., 2022). Dual-linker MIL-53(Al)-BDC/LA (85:15) exhibited ~15–18 % LA degradation, while dual-linker MIL-53 (Al)-BDC/LA (70:30) displayed a more pronounced LA degradation step of ~27–30 %. These observations demonstrate the successful integration of lauric acid into the MIL-53(Al)-BDC/LA framework, with the extent of LA-related weight loss increasing with its content. Yet, attempts to incorporate more than 30 % lauric acid into the framework were unsuccessful, likely due to steric hindrance from the bulky aliphatic tail of LA, which disrupts the coordination environment and prevents orderly framework formation. Moreover, LA's low affinity for the Al metal centers, compared to the aromatic BDC linker, further restricts its inclusion beyond a certain threshold. Thus, 30 % LA content appears to represent the upper limit for stable dual-linker insertion in this system. Finally, the third weight loss, around 40 % and 30 %, is attributed to the breakdown of the BDC-based framework occurs near 450–605 °C for variants (85:15) and (70:30), respectively. The inorganic aluminum oxide (Al_2O_3) residue persisted thermally stable across the entire temperature range and accounted for approximately 40–50 % of the final mass for all three MOFs.

3.1.4. SEM

The surface morphology and particle size distribution of the synthesized MOFs were examined using SEM, and the results are illustrated in Fig. 3. The SEM image of pristine MIL-53(Al), shown in Fig. 3(a) synthesized using terephthalic acid as the sole organic linker. The particles appear relatively uniform, with irregular polygonal and platelet-like morphologies. The particle size is generally small and well-dispersed, indicating good crystallinity and a high degree of nucleation under the synthesis conditions, which is in good accordance with the literature (Moinfar, Khodayari, Sami, et al., 2022b), which is assigned to the generation of pristine MIL-53(Al). Fig. 3(b) depicts the dual-linker MIL-53(Al) with a 0.85:0.15 M ratio of terephthalic acid to lauric acid. A noticeable increase in particle size and aggregation is observed compared to the pristine Al-MOF. The morphology becomes more heterogeneous, with larger, block-like agglomerates intermixed with finer particles. This could be due to the incomplete distribution of the long-chain linker in the framework formation, which disrupts the uniform growth of the MIL-53(Al) framework, introduces steric hindrance, and alters the self-assembly process. Fig. 3(c) corresponds to the dual-linker MIL-53(Al) synthesized using 70 % terephthalic acid and 30 % lauric acid. In this case, the morphology partially reverts toward that of the pristine MOF, with a finer distribution of particles and reduced agglomeration compared to the dual-linker (85:15) variant. Although irregular and broken fragments still indicate structural perturbation due to lauric acid inclusion, though to a lesser extent. This observation suggests that the synthesis and integration of the LA linker into the structure was successful and supports better framework integrity and controlled crystal growth.

3.1.5. Brunauer–emmett–teller (BET) analysis

The N_2 adsorption-desorption isotherm of pure MIL-53(Al) and its dual-linker versions was measured at 77 K to acquire a better understanding of their surface area and textural characteristics, as shown in Fig. 3(d) and Table S7. All three MOFs display Type IV isotherms, which are typical of mesoporous structures (Cevallos-Mendoza et al., 2024). The pure MIL-53(Al) has a surface area of 867 m^2/g, comparable to those described in the literature (Górtazar et al., 2025). The dual-linker variants, MIL-53(Al)-BDC/LA (85:15) and (70:30), have surface areas of 722 m^2/g and 571 m^2/g, respectively. The BJH pore size distribution curves demonstrate mesoporosity as found in Fig. S3, with a significant change in pore diameter and volume based on LA content. The pristine MIL-53(Al) has a total pore volume of 0.17 cm^3/g and a mean pore width of 1.22 nm, exhibiting microporous to mesoporous properties. The 85:15 variant had the same mean pore width (1.22 nm) but a higher pore volume (0.57 cm^3/g), indicating partial filling of pores. The 70:30 dual-linker variant exhibits a significant increase in mean pore width to 5.3 nm and pore volume of 0.74 cm^3/g, suggesting the formation of larger mesopores that led to structural expansion caused by increased LA content in the synthesis of dual-linker MIL-53(Al), as indicated by the BJH data of pore properties given in Table S7.

3.2. Response surface methodology of bisphenols extraction optimization

An RSM (Response Surface Methodology) model was developed and implemented using a CCD to optimize key parameters influencing the extraction process. These parameters included three numerical variables: sample volume, desorption solvent volume, and pH, and one categorical variable: desorption solvent type. All were found to significantly impact both extraction efficiency and enrichment factor. The selected parameters and their corresponding levels are presented in Table S1. A total of 54 experimental runs were conducted and detailed in Table S2. This design enables accurate estimation of main effects and interactions while ensuring consistent prediction variance throughout

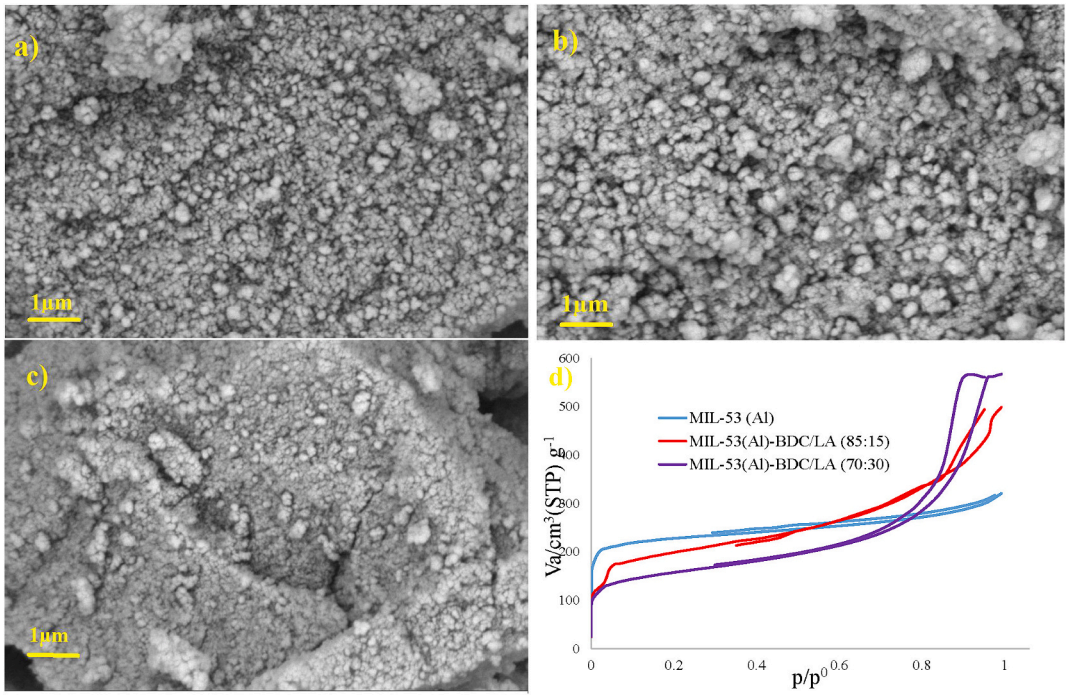

Fig. 3. SEM images of synthesized MOFs, (a) MIL-53(Al), (b) dual-linker MIL-53(Al)-BDC/LA (85:15). (c) dual-linker MIL-53(Al)-BDC/LA (70:30), and (d) BET scheme of the synthesized materials. MIL-53(Al) with pore volume 0.17 cm^3/g and surface area of 867.04 m^2/g, dual-linker MIL-53(Al)-BDC/LA (85:15) with pore volume 0.57 cm^3/g and surface area of 722.17 m^2/g, dual-linker MIL-53(Al)-BDC/LA (70:30) with pore volume 0.74 cm^3/g and surface area of 571.59 m^2/g.

the design space. The CCD demonstrated strong predictive capability for optimizing the extraction of bisphenol compounds. As shown in Table S3, the predicted and adjusted R^2 values were closely aligned across all three bisphenols, indicating a reliable model fit. Adequate precision values were notably high, 222.887 for BPF, 190.530 for BPA, and 131.530 for BPAF, further supporting the model's robustness. Reduced cubic models were fitted to the data, and analysis of variance (ANOVA) confirmed that all models were highly significant ($p < 0.0001$), while lack-of-fit was not significant ($p > 0.17$), indicating a good fit (see Tables S4–S6).

Specifically, the model for bisphenol F was exceptionally predictive, with an F-value of 3592.92 and an R^2 of 0.9998, accounting for 99.98 % of the variance. Similarly, bisphenol A's model had an F-value of 2571.96 and R^2 of 0.9997, while bisphenol AF showed an F-value of 1123.30 with an R^2 of 0.9993, all highly significant ($p < 0.0001$).

As illustrated in Fig. 4, desorption solvent volume (Factor C) emerged as the most influential parameter, producing extremely high F-values—40,908 for BPF, 26,941 for BPA, and 12,234 for BPAF (all $p < 0.0001$). A sufficient volume is required to fully wet and penetrate the sorbent, ensuring complete desorption of the analyte retained within its structure. However, excessive solvent volumes lead to dilution of the desorbed analytes, resulting in reduced signal intensity (Moinfar et al., 2025). In this study, poor repeatability was observed by using 100.0 μL, even though it provided the highest signal. Therefore, 150.0 μL was selected as the optimal volume, as it covers the entire sorbent, resulting in maximum desorption of the target bisphenols retained in the dual-linker MIL-53(Al). At this level, peak responses exceeded 4.0×10^6 for BPF, 8.6×10^6 for BPA, and 2.9×10^6 for BPAF, suggesting that minimal solvent use enhances extraction efficiency and analyte concentration.

Sample volume (Factor B) also played a crucial role. Increasing the sample volume, while keeping the analyte concentration constant, allows a greater total mass of analyte to interact with and be retained on the sorbent. This results in improved analyte enrichment and enhances the overall extraction performance (Moinfar et al., 2025; Moinfar, Khodayari, Abdulrahman, et al., 2022). Although 45.0 mL resulted in the highest responses in this study, it extended the processing time. Therefore, a slightly reduced volume of 38.0 mL was chosen as optimal, offering high recovery while improving efficiency. The corresponding F-values were 34,142 for BPF, 26,312 for BPA, and 13,055 for BPAF (all $p < 0.0001$).

Desorption solvent type (Factor *D*) was another significant factor ($F = 2559$ for BPF, 1608 for BPA, and 1178 for BPAF; all $p < 0.0001$). A mixture of acetonitrile and methanol consistently outperformed individual solvents, particularly for BPA and BPAF, because it provided the highest desorption efficiency, likely due to their complementary solvation properties. The target analytes are moderately polar, so a mixture of acetonitrile, a polar aprotic solvent, and methanol, a polar protic solvent, achieves a more balanced polarity capable of weakening π–π interactions and disrupting hydrogen bonding between the target bisphenols and the sorbent material (Hazra & Sarkar, 2002; Moinfar, Khodayari, Abdulrahman, et al., 2022; Skans et al., 2025b). pH (Factor A) had a moderate yet statistically significant effect, with pH 6.75 yielding the highest extraction efficiency. Possibly due to the deprotonation of the target bisphenols at pH values above 7, where they begin to acquire a negative charge based on their pKa values (Regueiro et al., 2015). Simultaneously, MIL-53(Al) has a point of zero charge (pHzpc) at 7.1 (Skans et al., 2025c), meaning its surface also becomes negatively charged above this pH. As a result, electrostatic repulsion occurs between the negatively charged bisphenols and the sorbent surface, and the hydrogen bonding disappears, reducing adsorption efficiency (Quan et al., 2020; G. Zhang, Wo, Sun, Hao, et al., 2021). In contrast, at pH values below 7, the target bisphenols remain in their neutral form, while the sorbent is positively charged. Under these conditions, electrostatic attraction is minimal or absent. Nevertheless, other non-covalent interactions such as π–π stacking, hydrogen bonding, and van der Waals forces become the dominant mechanisms facilitating the adsorption of the target bisphenols onto the dual-linker MIL-53(Al) framework (Zhou et al., 2013). Several interaction terms were significant, especially sample volume × solvent volume (BC) and solvent volume × solvent type (CD), emphasizing the necessity of multi-factor optimization. The significance of quadratic terms, particularly C^2, further confirmed that both excessively high and low solvent volumes impaired performance,

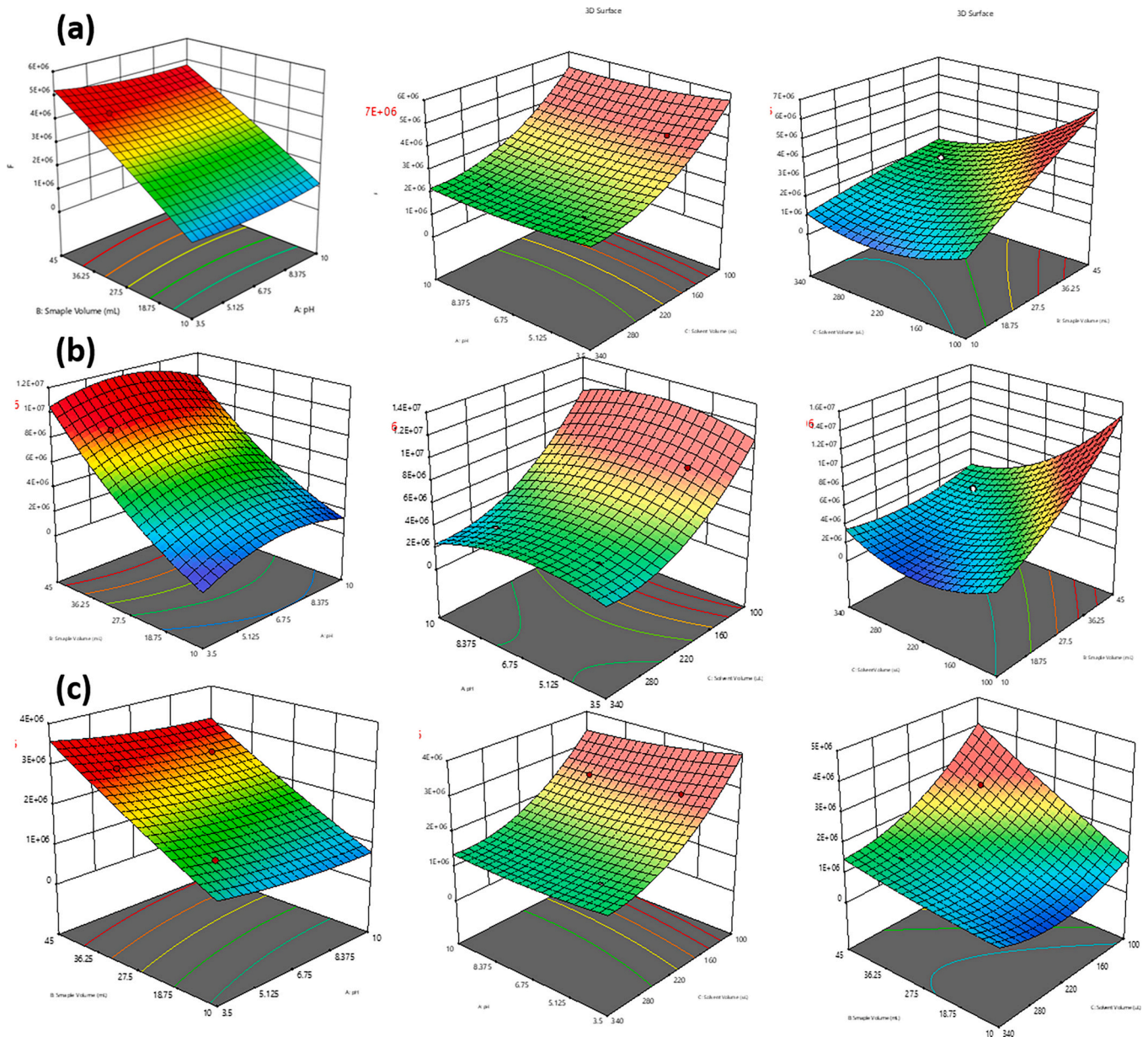

Fig. 4. Response surface analysis 3D diagram of (a) bisphenol F, (b) bisphenol A, (c) bisphenol AF.

because 100.0 μL results in poor repeatability, while excessive volumes lead to a decline in extraction efficiency and enrichment factor. Validating 150.0 μL as the optimal condition.

In summary, the study demonstrates that the most effective extraction of bisphenols is achieved using low solvent volumes, sample volumes, neutral pH, and a mixed acetonitrile-methanol solvent system.

3.3. Comparison of the prepared MIL-53(Al) and its variants

The extraction efficiency of pristine MIL-53(Al) and its dual-linker derivatives incorporating varying ratios of terephthalic acid and lauric acid was evaluated using chromatographic analysis under the same experimental conditions. The corresponding chromatograms for MIL-53 (Al) and its modified bi-ligands are shown in Fig. 6 (A).

Among the tested materials, the dual-linker MIL-53(Al)-BDC/LA (70:30) exhibited the highest extraction efficiency for all three bisphenols. This enhancement in performance can be attributed to the changed physicochemical properties of the framework. Specifically, the partial substitution of terephthalic acid with lauric acid modulates the hydrophobicity and pore environment of the MOF (Choi et al., 2011). The 30 % lauric acid variant achieves a favorable balance between the rigid, aromatic characteristics of terephthalic acid, critical for π–π interactions between the aromatic rings of bisphenols and the terephthalic acid linkers, and the hydrophobic nature of lauric acid, which enhances van der Waals interactions with the largely hydrophobic bisphenol molecules (H. Li et al., 2023). Moreover, Hydrogen bonding occurs between the hydroxyl groups of bisphenols and the carboxylate or hydroxyl sites within the framework. The FTIR spectra in Fig. 5 confirm the claims by providing the data of dual-linker MIL-53(Al)-BDC/LA (30 %) before and after treatment with BPA. The spectrum displays the O—H stretching vibration bands at around 3100–3400 cm^{-1}. These bands intensified upon the adsorption of BPA, particularly at 5 mg/L, indicating an increase in the hydrogen bonding interaction due to the presence of adsorbed molecules containing O—H groups (Gao et al., 2019). Additionally, pristine MIL-53(Al), composed entirely of BDC linkers, shows lower extraction efficiency compared to the 30 % dual-linker variant of MIL-53(Al), reducing its affinity for bisphenol compounds, which are largely hydrophobic (Choi et al., 2011; Loganathan

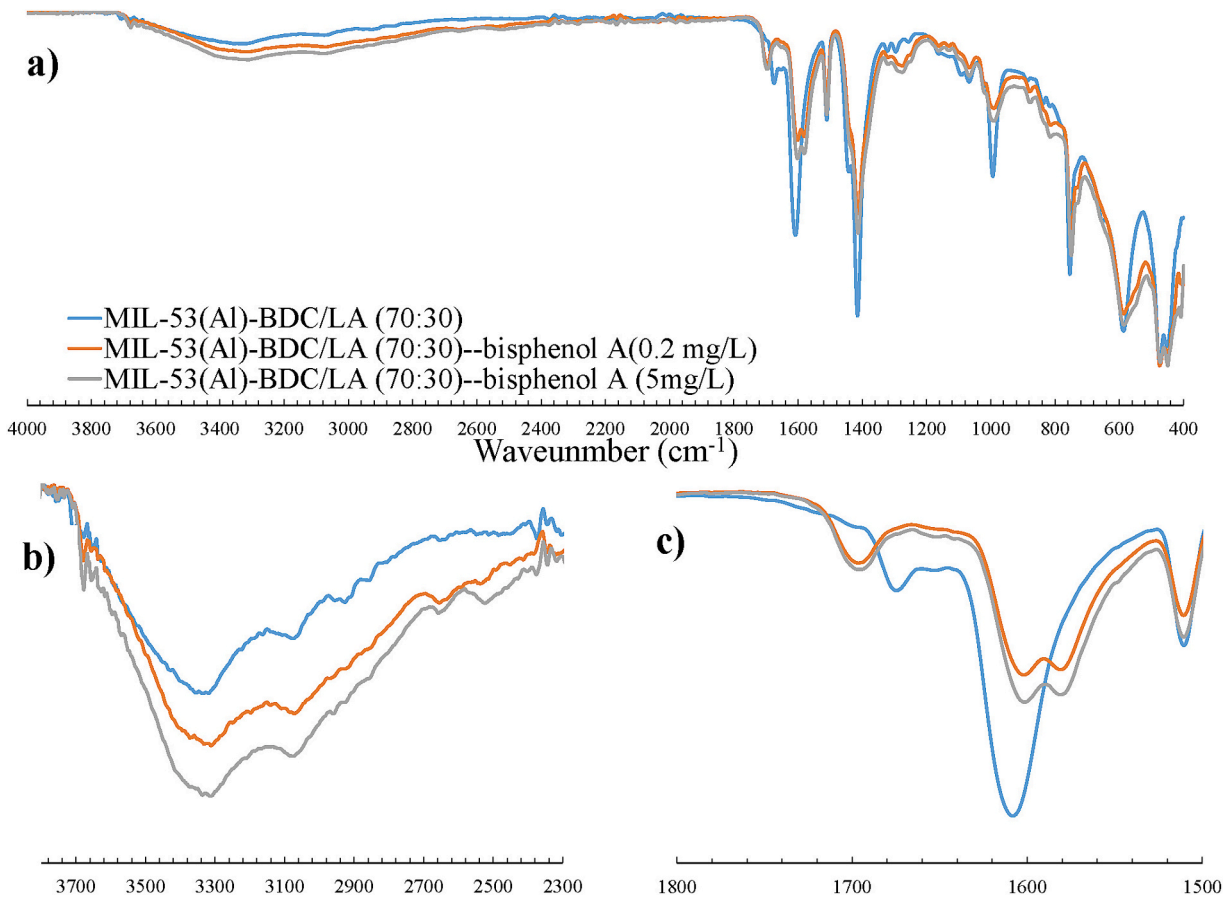

Fig. 5. FTIR spectra of (a) dual-linker MIL-53(Al)-BDC/LA before and after adsorption of bisphenol A at 0.2 mg/L and 5.0 mg/L. (b) H-bonding magnified region, (c) C═O and C═C region related to π–π interaction.

et al., 2023). The lack of alkyl functional groups further constrains the diversity of host–guest interactions, relying mainly on π–π stacking and hydrogen bonding (Luo et al., 2019). In contrast, the bi-linker MIL-53 (Al) materials incorporate both aromatic (terephthalic acid) and aliphatic (lauric acid) linkers, introducing a hybrid surface environment that promotes stronger and more diverse interactions with the bisphenols. As seen in Fig. 5, the asymmetric stretching band of the carboxylate group shifted from 1672 to 1700 cm^{-1} and the vibrational band attributed to aromatic C═C stretching of the terephthalate linker around 1600–1620 cm^{-1} was shifted to 1570–1620 cm^{-1} as a two-peak shape and changes in intensity, after the adsorption of BPA, suggesting strong π–π stacking interactions and electrostatic attractions between the aromatic rings of BPA and the phenyl moieties of the MOF (Valenzuela et al., 2025). This synergistic enhancement of hydrophobicity and chemical functionality is absent in the pristine MOF, which accounts for its comparatively lower adsorption performance. Notably, bisphenol A (BPA) yielded the highest signal intensity across all tested materials. This trend likely results from BpA's molecular structure, which features two methyl-substituted phenolic rings. These confer higher hydrophobicity and greater propensity for π–π stacking interactions compared to BpF and BpAF (H. Li et al., 2023). It is noteworthy that the 30 % dual-linker variant was synthesized repeatedly and consistently yielded comparable performance, indicating good reproducibility. Although a 50 % variant was also prepared, it did not exhibit satisfactory characteristics and was therefore not further pursued. When comparing the 15 % and 30 % dual-linker MOFs with the pristine MOF, BET analysis revealed that the 15 % composition possessed a higher surface area but a lower pore volume relative to the 30 % counterpart, having a higher ratio of LA linker. While pristine MOF exhibited the lowest pore volume due to the sole 1,4-BDC linker. Moreover, SEM analysis illustrated pronounced agglomeration and heterogeneous particle distribution in the 15 % variant, whereas the 30 % variant displayed more uniform morphology and improved particle dispersion relatively same as pristine MOF. Overall, the incorporation of 30 % lauric acid into MIL-53(Al) significantly improves the framework's affinity for bisphenols adsorption, making it a promising candidate for environmental and analytical applications targeting endocrine-disrupting compounds.

3.4. Method validation

The performance of the dual-linker MIL-53(Al)-BDC/LA (70:30)-PT-μSPE/HPLC-PDA technique was evaluated using key analytical parameters such as limit of detection (LOD), limit of quantification (LOQ), enrichment factor (EF), relative standard deviation (RSD%), correlation coefficient (r^2), and linearity range for bisphenols A, F, and AF. Table 1 displays the method validation. LOD and LOQ values were determined based on signal-to-noise ratios of 3 and 10, respectively. Calibration curves were constructed for each analyte over a concentration range from 0.01 to 200.0 μg/L, achieving correlation coefficients (r^2) between 0.9899 and 0.9996, indicative of excellent linearity. Method precision was evaluated through five replicate analyses at two concentration levels (30.0 and 80.0 μg/L) for each bisphenol. Inter-day precision was further assessed over three consecutive days with the same sorbent material. The method demonstrated excellent repeatability, with RSD% values not exceeding 7 % for any of the target bisphenols, confirming its robustness and reliability. The enrichment factors for bisphenols F, A, and AF were 126, 176, and 209, respectively, underscoring the effectiveness of the preconcentration step in enhancing the method's sensitivity.

Table 1
Analytical performance of PT-μ-SPE /HPLC-PDA methods in water samples.

	LOD[a]	LOQ[b]	r^2 [c]	LR[d]	EF[e]	RSD%(intra-day)[f]		RSD%(inter-day)[g]	
	(μg/L)	(μg/L)				30.0 (μg/L)	80.0 (μg/L)	30.0 (μg/L)	80.0 (μg/L)
BpF	0.1	0.4	0.9996	0.33–200	126.6	4.0	5.2	5.0	6.6
BpA	0.03	0.1	0.9955	0.099–200	176.0	3.5	4.0	4.2	4.9
BpAF	0.01	0.04	0.9899	0.03–200	209.5	5.8	4.7	7.0	6.0

[a] Limit of detection ($S/N = 3$) (μg/L).
[b] Limit of quantification (S/N = 10) (μg/L).
[c] Coefficient of determination.
[d] Linear range (μg/L).
[e] Enrichment factor (μg/L).
[f] Relative standard deviation at a concentration of 30.0 and 80.0 μg/L of each analyte for intra-day ($n = 5$).
[g] Relative standard deviation at a concentration of 30.0 and 80.0 μg/L of each analyte for inter-day ($n = 3$).

3.5. Real sample analysis and matrix effect

For the evaluation of the applicability of the proposed synthesized MOF as a sorbent in PT-μSPE for bisphenol extraction, various food products and packaging materials were selected as real samples, including tea in disposable cups, instant noodles, polyethylene terephthalate (PET) water bottles, disposable containers, and cups. These samples were spiked with different concentrations of the target bisphenols and subsequently processed using pipette tips with dual-linker MIL-53(Al)-BDC/LA (70:30) as sorbent material and analyzed

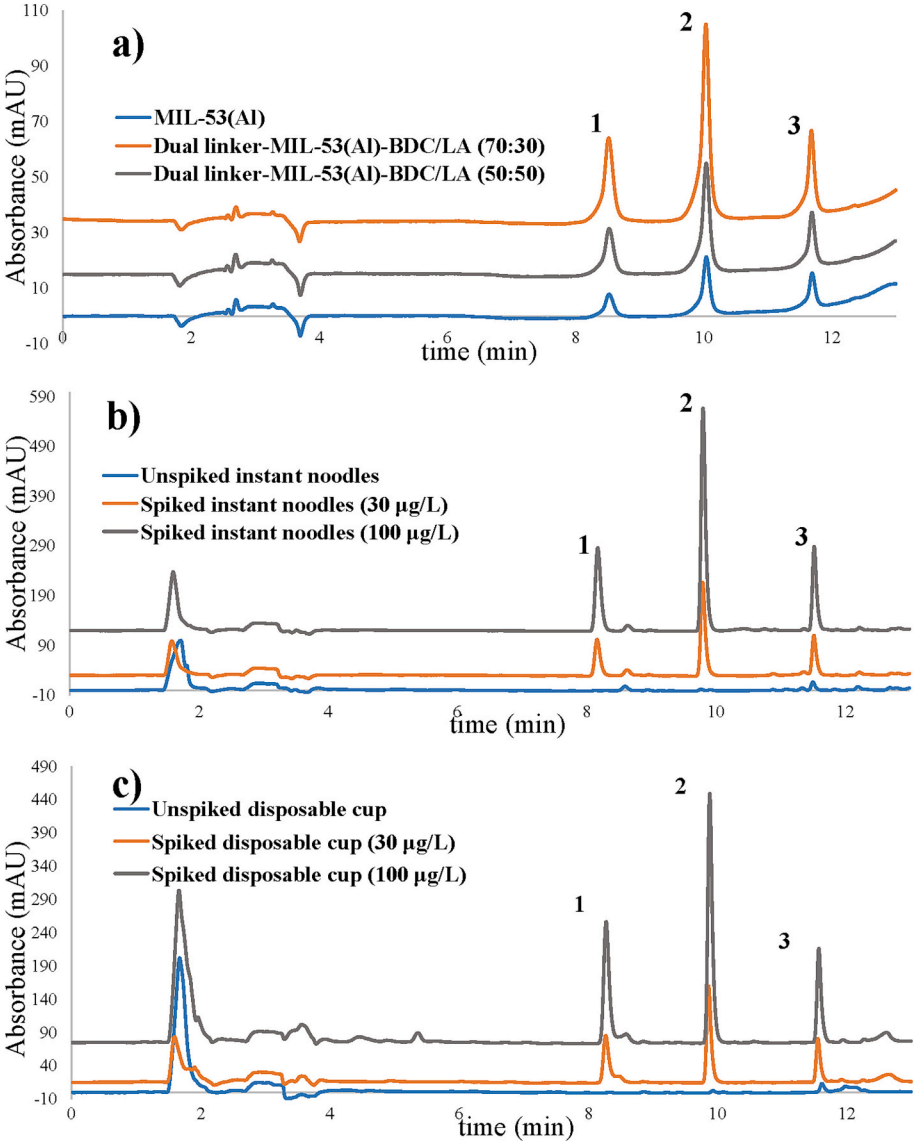

Fig. 6. Representative HPLC-PDA chromatograms of (a) comparing MOF samples, all experiments were performed under identical conditions: concentration of Bisphenols (0.5 mg/L), Sample volume (10.0 mL), solvent volume (500.0 μL), pH 6. Real sample analysis of (b) Instant noodles, (c) Disposable cup, using dual-linker MIL-53(Al)-BDC/LA (70:30) as sorbent under optimized conditions for the extraction of 1: BPF, 2: BPA, and 3: BPAF.

by HPLC-PDA. Representative chromatograms of non-spiked and spiked samples at two concentration levels (30.0 and 100.0 μg/L) for the PET water bottle, tea, and disposable cup are presented in Fig. S2. As for the disposable cup and instant noodles, they are shown in Figs. 6 (B and C). The corresponding relative recoveries (RR%) and matrix effect (ME%) across different real sample types are summarized in Table 2. These evaluations reflect the method's accuracy in real sample matrices. The matrix effect (ME%) was evaluated by comparing the analytical responses of bisphenols in real samples with those in ultrapure water. It was calculated using the following equation:

$$ME\% = \frac{(A_s - A_n)}{Aw} \times 100 \quad (3)$$

where A_s is the peak area of the analyte in the spiked sample, A_n is the peak area in the non-spiked (blank) sample, and A_w is the peak area in the spiked ultrapure water.

Table 2
Relative recoveries and matrix effect estimation of the proposed method for the determination of BpF, BpA, and BpAF in real samples.

Samples	Compounds	Added (μg/L)	Found (μg/L)	RR%	ME%
	BpF	0	n.d	–	
		30.0	29.6	98.5	
		100.0	99.0	99.0	98.2
PET water bottles					
	BpA	0	<LOQ	–	
		30	27.3	91.0	
		100	96.5	96.5	95.3
	BpAF	0	2.8	–	
		30	27.7	83.0	
		100	102.6	99.8	99.0
	BpF	0	n.d		
		30	23.5	78.0	
		100	86.3	86.32	89.6
Tea					
	BpA	0	<LOQ	–	
		30	25.3	84.0	
		100	89.4	89.4	86.04
	BpAF	0	<LOQ		
		30	24.6	82.0	
		100	93.7	93.7	87.4
	BpF	0	n.d		
		30	26.5	88.4	
		100	90.3	90.30	93.3
Instant noodles					
	BpA	0	<LOQ	–	
		30	25.4	84.6	
		100	89.9	89.9	97.14
	BpAF	0	2.3	–	
		30	28.7	87.8	
		100	98.7	96.4	98.3
	BpF	0	n.d	–	
		30	26.2	87.3	
		100	92.8	92.8	97.7
Plastic container					
	BpA	0	<LOQ	–	
		30	27.5	91.6	
		100	97.8	97.8	98.4.03
	BpAF	0	3.5		
		30	28.7	84.0	
		100	98.7	95.4	98.8
	BpF	0	n.d	–	
		30	26.3	87.6	
		100	93.4	93.4	93.5
Plastic cup					
	BpA	0	<LOQ	–	
		30	24.8	82.8	
		100	99.4	99.4	97.2
	BpAF	0	2.5	–	
		30	28.3	86.0	
		100	94.4	91.9	91.4

n.d: not detect. <LOQ: founded amount less than LOQ.

3.6. Method performance evaluation

Table 3 summarizes the comparative evaluation of the PT-μSPE method utilizing dual-linker MIL-53(Al)-BDC/LA (70:30) as sorbent material, representing its superior performance for target bisphenols determination by HPLC-PDA relative to previously reported methods in terms of linear ranges, sorbent quantity, solvent and sample volume, limits of detection, and EF. The presented method achieves a low LOD of 0.01–0.1 μg/L, comparable to or better than many existing techniques, such as MSPE-HPLC-FLD with MIP-MCOF and $CoFe_2O_4$/NOM/graphene. Additionally, the proposed method offers a wide linear range (0.04–200.0 μg/L) and excellent enrichment factor (EF = 126–209), surpassing those listed in other studies, including DSPE-HPLC-UV/VIS and MSPE-HPLC-FLD with MIP-MCOF. PT-μSPE uses a moderate sorbent amount (20.0 mg) and processes a considerably larger sample volume (38.0 mL) than MIP-MCOF (5.0 mL) and $CoFe_2O_4$/NOM/graphene (10.0 mL), enabling improved representativeness without increasing material consumption. Its solvent requirement (150.0 μL) is lower than the 1000.0 μL needed for $CoFe_2O_4$/NOM/graphene and comparable to the 100.0 μL used in the MIP-MCOF method, offering a greener and more economical extraction. Although its extraction time (20.0 min) is longer than the time required for the other methods, this is offset by the much higher sample throughput per run and its strong enrichment capability. Relative to other reported approaches, including (Fe_3O_4@TAPB-COF@ZIF-8) in the MSPE method, (ZIF-7@ZIF-67/PES) in the DSPE, and ($CoFe_2O_4$@NH_2@COF) in the mSBSD-ME technique, the PT-μSPE method shows a more favorable trade-off between operational simplicity and analytical performance. Methods such as DSPE and graphene-modified sorbents require larger amounts of organic solvent (500.0–1000.0 μL), while mSBSD-ME employs very small sample volumes unsuitable for routine monitoring. Furthermore, the method demonstrates good precision of intra-day with relative standard deviations (RSD%) < 5.8. Moreover, a mechanistic and practical comparison of the synthesized dual-linker MOF with the referenced sorbent materials is provided in Table S8. Overall, the dual-linker MOF-based PT-μSPE exhibits markedly improved performance, offering a more sensitive, reproducible, and operationally efficient approach for the determination of target bisphenols in food samples and packaging.

3.7. Conclusion

Although MOFs have been investigated as adsorbents in μSPE methods for the analysis of trace analytes such as bisphenol A in complex matrices in many studies, researchers are still looking for adsorbents with higher selectivity and extraction efficiency. Although MIL-53 (Al) has a high surface area, in this study, adding 30 % lauric acid as a secondary binder to the MIL-53(Al) structure significantly enhanced the adsorbent performance by tuning the pore hydrophobicity and surface chemistry. A micro-pipette tip solid phase extraction (PT-μSPE) method using the dual binder MIL-53(Al)-BDC/LA (70:30) as the adsorbent in combination with HPLC-PDA was successfully developed and validated for the extraction and determination of bisphenols in food and packaging samples. As a result, the MIL-53(Al)-BDC/LA (70,30) adsorbent significantly improved the extraction efficiency and sensitivity

Table 3
Comparison of the performance of the extraction methods for bisphenols detection between the present method and previous studies in the literature.

Methods	Sorbents	analyte	Sample matrix	Sorbent Amount (mg)	Sample volume (mL)	Organic solvent (μL)	Time (min)	LOD (μg/L)	Linear range (μg/L)	RSD%	EF	Reference
MSPE-HPLC-FLD	MIP-MCOF	BPA	Barreled/river/tap water Beverages/Human urine	15.0	5.0	100.0	5.0	0.02	0.1–100	0.5–5.7	34.8–45.7	(Xiang et al., 2023)
MSPE-HPLC-DAD	Fe3O4@TAPB-COF@ZIF-8	BPA, BPB, PBAP,BPBP	Plastic-packaged bevarages.	25.0	20.0	200.0	20.0	0.04–0.05	0.25–1000	1.2–4.3	—	(H. L. Jiang et al., 2021b)
MSPE-HPLC-FLD	CoFe2O4/NOM/graphene	BPA	synthetic samples, bottled water, municipal supply water, and environmental water	50.0	10.0	1000.0	5.0	0.022	0.1–5000	2.13–2.21	—	(Oliveira et al., 2022)
DSPE-HPLC-UV/VIS	ZIF-7@ZIF-67/PES composite	BPA, BPh	Frozen water in PET bottle, Baby milk bottle, and thermal paper	15.0	20.0	500.0	20.0	0.6	2–500	<3.1	150	(Amareh et al., 2023)
mSBSD-ME-LC-MS/MS	CoFe2O4@NH2@COF	BPA,BPB,BPAP, BPF,BPS,BPE, BPC,BPS,BPZ	follicular fluid samples	0.5	0.35	20.0	1.0	0.01–0.08	≤50	≤11.5	8.5–14.3	(Vállez-Gomis et al., 2024)
PT-μSPE-HPLC-PDA	Dual-linker MIL-53(Al)-BDC/LA (70:30)	BPA, BPF, BPAF	PET water bottle, instant noodles, plastic container, tea, plastic cups.	20.0	38.0	150.0	20.0	0.01–0.1	0.04–200	<5.8	126.6–209.5	This work

MSPE: Magnetic solid-phase extraction.
DSPE: Dispersive solid-phase extraction.
mSBSD-ME: miniaturized stir bar sorptive dispersive microextraction.
PT-μSPE: Pipette tip-micro solid-phase extraction.

compared with the original MIL-53(Al) and MIL-53(Al)-BDC/LA (85,15). The PT-μSPE/HPLC-PDA method showed excellent analytical performance, including low detection limits, wide linear range, and satisfactory intra- and inter-day precision (RSD $\leq$ 7 %). These results confirm the robustness, reproducibility, and suitability of the developed approach for monitoring target bisphenols at low levels in complex food matrices. Despite its advantages, the back pressure generated at the pipette tip during operation poses a practical limitation that can impede sample flow and affect reproducibility. Future studies should explore modified packaging strategies, different adsorbent designs, or improved tip designs to minimize flow resistance and increase operational stability. Future research should also explore the incorporation of hydrophobic or functionalized ligands to increase selectivity toward a broader range of endocrine-disrupting compounds.

CRediT authorship contribution statement

Helan Zeyad Sami: Writing – review & editing, Writing – original draft, Resources, Methodology, Investigation, Conceptualization. **Lazgin Abdi Jameel:** Supervision, Resources, Investigation, Funding acquisition. **Soleiman Moinfar:** Writing – review & editing, Supervision, Resources, Project administration, Methodology, Conceptualization.

Declaration of competing interest

The authors declare that they have no known competing financial interests or personal relationships that could have appeared to influence the work reported in this paper.

Acknowledgement

The authors gratefully acknowledge the financial support provided by the University of Zakho for this work.

Appendix A. Supplementary data

Supplementary data to this article can be found online at https://doi.org/10.1016/j.foodchem.2025.147681.

Data availability

No data was used for the research described in the article.

References

Ahmed, H. E. H., Aliyev, E., Alosmanov, R., & Soylak, M. (2025). Separation and enrichment of cd and pb from food and water samples based on a graphene oxide-decorated poly 2-diethylaminoethyl methacrylate nanocomposite by dispersive micro-solid phase extraction (d-μ-SPE). *Food Chemistry, 465*, Article 142008. https://doi.org/10.1016/J.FOODCHEM.2024.142008

Amareh, N., Yamini, Y., Saeidi, M., Dinmohammadpour, Z., & Nazraz, M. (2023). Synthesis, characterization and application of ZIF-7@ZIF-67/PES for dispersive solid phase extraction of bisphenol A and 2-phenyl phenol. *Talanta Open, 8*, Article 100269. https://doi.org/10.1016/J.TALO.2023.100269

Carrington, E. J., Pétuya, R., Hylton, R. K., Yan, Y., Antypov, D., Darling, G. R., … Rosseinsky, M. J. (2019). The anisotropic responses of a flexible metal-organic framework constructed from asymmetric flexible linkers and heptanuclear zinc carboxylate secondary building units. *Crystal Growth and Design, 19*(10), 5604–5618. https://doi.org/10.1021/ACS.CGD.9B00558/SUPPL_FILE/CG9B00558_SI_002.ZIP

Catron, T. R., Keely, S. P., Brinkman, N. E., Zurlinden, T. J., Wood, C. E., Wright, J. R., … Tal, T. (2019). Host developmental toxicity of BPA and BPA alternatives is inversely related to microbiota disruption in zebrafish. *Toxicological Sciences, 167*(2), 468–483. https://doi.org/10.1093/TOXSCI/KFY261

Cevallos-Mendoza, J. E., Cedeño-Muñoz, J. S., Navia-Mendoza, J. M., Figueira, F., Amorim, C. G., Rodríguez-Díaz, J. M., & Montenegro, M. C. B. S. M. (2024). Development of hybrid MIL-53(Al)@CBS for ternary adsorption of tetracyclines antibiotics in water: Physical interpretation of the adsorption mechanism. *Bioresource Technology, 396*, Article 130453. https://doi.org/10.1016/J.BIORTECH.2024.130453

Chen, D., Kannan, K., Tan, H., Zheng, Z., Feng, Y. L., Wu, Y., & Widelka, M. (2016). Bisphenol analogues other than BPA: Environmental occurrence, human exposure,

and toxicity - A review. *Environmental Science and Technology, 50*(11), 5438–5453. https://doi.org/10.1021/ACS.EST.5B05387/SUPPL_FILE/ES5B05387_SI_001.PDF

Chen, M., Gao, S., Liu, R., Wang, X., Nie, C., Xie, F., Gao, H., & Wan, L. (2025). Imprinted metal-organic framework for selective extraction and determination of fluoroquinolone antibiotics in food samples. *LWT, 223*, Article 117743. https://doi.org/10.1016/J.LWT.2025.117743

Choi, K. M., Jeon, H. J., Kang, J. K., & Yaghi, O. M. (2011). Heterogeneity within order in crystals of a porous metal-organic framework. *Journal of the American Chemical Society, 133*(31), 11920–11923. https://doi.org/10.1021/JA204818Q/SUPPL_FILE/JA204818Q_SI_001.PDF

Ding, Y., Feng, J., Sun, M., Feng, Y., Xin, X., & Sun, M. (2024). Extraction improvement of ionic liquid-functionalized silica by in situ anion-exchange for online solid-phase extraction of estrogens in honey. *Food Chemistry, 445*, Article 138706. https://doi.org/10.1016/J.FOODCHEM.2024.138706

Escher, A., Megahd, H., Tavella, C., Comoretto, D., & Lova, P. (2023). Colorimetric polymer sensors for smart packaging. *Macromolecular Chemistry and Physics, 224*(14), 2300022. https://doi.org/10.1002/MACP.202300022;PAGE:STRING:ARTICLE/CHAPTER

Gandomkar, F., Khajeh, M., Oveisi, A. R., Karimi, P., & García, H. (2025). Preparation of a novel porous organic polymer for selective extraction/determination of palladium ions from water samples. *Polymer, 316*, Article 127858. https://doi.org/10.1016/J.POLYMER.2024.127858

Gao, M., Liu, W., Wang, X., Li, Y., Zhou, P., Shi, L., … Wang, X. (2019). Hydrogen-bonding-induced efficient dispersive solid phase extraction of bisphenols and their derivatives in environmental waters using surface amino-functionalized MIL-101 (Fe). *Microchemical Journal, 145*, 1151–1161. https://doi.org/10.1016/J.MICROC.2018.12.013

Górtazar, G., Fernández-González, D., Montoro, C., Romero, J. F., Dafinov, A., Jiménez, A., … López-Maya, E. (2025). Holistic green synthesis at room temperature of MIL-53(Al) from aluminum slag and application for glucose conversion to 5-hydroxymethylfurfural. *Sustainable Chemistry and Pharmacy, 46*, Article 102060. https://doi.org/10.1016/J.SCP.2025.102060

Gupta, R. K., Pipliya, S., Karunanithi, S., Eswaran, U. G. M., Kumar, S., Mandliya, S., … Kovács, B. (2024). Migration of chemical compounds from packaging materials into packaged foods: interaction, mechanism, assessment, and regulations. *Foods* (Vol. 13,(19), 3125. https://doi.org/10.3390/FOODS13193125

Ha, H., Hahm, H., Jwa, D. G., Yoo, K., Park, M. H., Yoon, M., … Kim, M. (2017). Flexibility in metal–organic frameworks derived from positional and electronic effects of functional groups. *CrystEngComm, 19*(36), 5361–5368. https://doi.org/10.1039/C7CE00971B

Hazra, P., & Sarkar, N. (2002). Solvation dynamics of coumarin 490 in methanol and acetonitrile reverse micelles. *Physical Chemistry Chemical Physics, 4*(6), 1040–1045. https://doi.org/10.1039/B109447E

Jala, A., Varghese, B., Dutta, R., Adela, R., & Borkar, R. M. (2022). Levels of parabens and bisphenols in personal care products and urinary concentrations in Indian young adult women: Implications for human exposure and health risk assessment. *Chemosphere, 297*, Article 134028. https://doi.org/10.1016/J.CHEMOSPHERE.2022.134028

Jiang, H. L., Fu, Q. B., Wang, M. L., Lin, J. M., & Zhao, R. S. (2021a). Determination of trace bisphenols in functional beverages through the magnetic solid-phase extraction with MOF-COF composite. *Food Chemistry, 345*, Article 128841. https://doi.org/10.1016/J.FOODCHEM.2020.128841

Jiang, H. L., Fu, Q. B., Wang, M. L., Lin, J. M., & Zhao, R. S. (2021b). Determination of trace bisphenols in functional beverages through the magnetic solid-phase extraction with MOF-COF composite. *Food Chemistry, 345*, Article 128841. https://doi.org/10.1016/J.FOODCHEM.2020.128841

Jiang, J., Zheng, Q., Yan, Y., Guo, D., Wang, F., Wu, S., & Sun, W. (2018). Design of a novel nanocomposite with C-S-H@LA for thermal energy storage: A theoretical and experimental study. *Applied Energy, 220*, 395–407. https://doi.org/10.1016/J.APENERGY.2018.03.134

Kamal, G. M., Anwar, I., Saadullah, K., Gere, A., Yasmin, S., Uddin, J., … Nayik, G. A. (2025). Extraction, quantification and health risk assessment of bisphenol A from various kinds of packaged milk and baby bottles. *Food Chemistry: X, 27*, Article 102387. https://doi.org/10.1016/J.FOCHX.2025.102387

Katugampalage, T. R., Ratanatawanate, C., Opaprakasit, P., Kaewsaneha, C., & Sreearunothai, P. (2021). A smart magnetically separable MIL-53(Al) MOF-coated nano-adsorbent for antibiotic pollutant removal with rapid and non-contact inductive heat regeneration. *Chemical Engineering Journal Advances, 8*, Article 100160. https://doi.org/10.1016/J.CEJA.2021.100160

Kaykhaii, M., Yavari, E., Sargazi, G., & Ebrahimi, A. K. (2020). Highly sensitive determination of bisphenol A in bottled water samples by HPLC after its extraction by a novel Th-MOF pipette-tip Micro-SPE. *Journal of Chromatographic Science, 58*(4), 373–382. https://doi.org/10.1093/CHROMSCI/BMZ111

Khan, M. J., Mookiah, S., Subramaniam, Y., & Ramiah, S. K. (2024). Effect of pullulan active packaging, incorporated with silver nanoparticles, on cholesterol oxidation product concentrations in boiler meat during storage. *Quality Assurance & Safety of Crops and Food, 16*(2), 81–88. https://doi.org/10.15586/QAS.V16I2.1454

Khan, S., Prasad, A., Filipe, C. D. M., & Didar, T. F. (2025). Smart food packaging for monitoring food quality. *Antimicrobial Food Packaging, Second Edition, 175–192*. https://doi.org/10.1016/B978-0-323-90747-7.00012-0

Lehmler, H. J., Liu, B., Gadogbe, M., & Bao, W. (2018). Exposure to Bisphenol A, Bisphenol F, and Bisphenol S in U.S. Adults and Children: The National Health and nutrition examination survey 2013-2014. *ACS Omega, 3*(6), 6523–6532. doi:10.1021/ACSOMEGA.8B00824/SUPPL_FILE/AO8B00824_SI_001.PDF.

Li, H., Lin, C., Ma, R., & Chen, Y. (2023). Π–π stack driven competitive /complementary adsorption of aromatic compounds on MIL-53(Al). *Chemosphere, 337*, Article 139377. https://doi.org/10.1016/J.CHEMOSPHERE.2023.139377

Li, S., Ma, J., Wu, G., Li, J., Wang, X., & Chen, L. (2022). Magnetic covalent-organic frameworks for the simultaneous extraction of eleven emerging aromatic disinfection byproducts in water samples coupled with UHPLC–MS/MS determination. *Journal of Hazardous Materials, 424*, Article 127687. https://doi.org/10.1016/J.JHAZMAT.2021.127687

Liao, C., & Kannan, K. (2013). Concentrations and profiles of bisphenol a and other bisphenol analogues in foodstuffs from the United States and their implications for human exposure. *Journal of Agricultural and Food Chemistry, 61*(19), 4655–4662. https://doi.org/10.1021/JF400445N/SUPPL_FILE/JF400445N_SI_001.PDF

Loganathan, P., Vigneswaran, S., Kandasamy, J., Nguyen, T. V., Katarzyna Cuprys, A., & Ratnaweera, H. (2023). Bisphenols in water: Occurrence, effects, and mitigation strategies. *Chemosphere, 328*, Article 138560. https://doi.org/10.1016/J.CHEMOSPHERE.2023.138560

López-Juan, A. L., Vállez-Gomis, V., Benedé, J. L., Martín-Esteban, A., & Chisvert, A. (2024). Bisphenols determination in seminal fluid by miniaturized stir bar sorptive dispersive microextraction as a potential tool in male infertility studies. *Microchemical Journal, 207*, Article 112222. https://doi.org/10.1016/J.MICROC.2024.112222

Luo, Z., Chen, H., Wu, S., Yang, C., & Cheng, J. (2019). Enhanced removal of bisphenol A from aqueous solution by aluminum-based MOF/sodium alginate-chitosan composite beads. *Chemosphere, 237*, Article 124493. https://doi.org/10.1016/J.CHEMOSPHERE.2019.124493

Lv, L., Liu, H., Wang, L., Wang, S., Li, Y., Zhang, G., & Zhao, Y. (2025). Metal-organic framework UiO-66-NH2 functionalized polydopamine-modified magnetic multi-walled carbon nanotubes for convenient magnetic solid-phase extraction of sixteen quinolones. *Food Chemistry, 486*, Article 144604. https://doi.org/10.1016/J.FOODCHEM.2025.144604

Majumder, M., Choudhary, R. B., Thakur, A. K., Khodayari, A., Amiri, M., Boukherroub, R., & Szunerits, S. (2020). Aluminum based metal-organic framework integrated with reduced graphene oxide for improved supercapacitive performance. *Electrochimica Acta, 353*, Article 136609. https://doi.org/10.1016/J.ELECTACTA.2020.136609

Martín-Gómez, B., Stephen Elmore, J., Valverde, S., Ares, A. M., & Bernal, J. (2024). Recent applications of chromatography for determining microplastics and related compounds (bisphenols and phthalate esters) in food. *Microchemical Journal, 197*, Article 109903. https://doi.org/10.1016/J.MICROC.2024.109903

Meng, W., Li, H., Wang, K., & Cao, Y. (2022). Determination of four bisphenols in plastic packaging beverages by ultrasonic-assisted dispersive liquid–liquid microextraction. *Packaging Technology and Science, 35*(10), 753–764. https://doi.org/10.1002/PTS.2677;PAGEGROUP:STRING:PUBLICATION

Michałowicz, J. (2014). Bisphenol A – Sources, toxicity and biotransformation. *Environmental Toxicology and Pharmacology, 37*(2), 738–758. https://doi.org/10.1016/J.ETAP.2014.02.003

Moinfar, S., Jamil, L. A., Sami, H. Z., & Ataei, S. (2021). An innovative continuous sample drop flow microextraction for GC–MS determination of pesticides in grape juice and water samples. *Journal of Food Composition and Analysis, 95*, Article 103695. https://doi.org/10.1016/J.JFCA.2020.103695

Moinfar, S., Khodayari, A., Abdulrahman, S. S., Aghaei, A., Sohrabnezhad, S., & Jamil, L. A. (2022). Development of a SPE/GC–MS method for the determination of organophosphorus pesticides in food samples using syringe filters packed by GNP/MIL-101(Cr) nanocomposite. *Food Chemistry, 371*, Article 130997. https://doi.org/10.1016/J.FOODCHEM.2021.130997

Moinfar, S., Khodayari, A., Mohammed, A. M., Pourbasheer, E., & Aghaei, A. (2025). NH2-MIL-101(Cr)/SBA15 nanocomposite as sorbent in syringe-filter-SPE for determination of pesticides in environmental water. *Microchemical Journal, 218*, Article 115322. https://doi.org/10.1016/J.MICROC.2025.115322

Moinfar, S., Khodayari, A., Sami, H. Z., Ali, M. K., & Abdi, N. N. (2022a). Investigation of five metal–organic frameworks as sorbents in the syringe filter-SPE method for determination of metronidazole and cephalexin in water samples. *New Journal of Chemistry, 46*(21), 10308–10316. https://doi.org/10.1039/D2NJ00907B

Moinfar, S., Khodayari, A., Sami, H. Z., Ali, M. K., & Abdi, N. N. (2022b). Investigation of five metal–organic frameworks as sorbents in the syringe filter-SPE method for determination of metronidazole and cephalexin in water samples. *New Journal of Chemistry, 46*(21), 10308–10316. https://doi.org/10.1039/D2NJ00907B

Noonan, G. O., Ackerman, L. K., & Begley, T. H. (2011). Concentration of bisphenol a in highly consumed canned foods on the U.S. market. *Journal of Agricultural and Food Chemistry, 59*(13), 7178–7185. doi:10.1021/JF201076F;JOURNAL:JOURNAL:JAFCAU;ISSUE:ISSUE:10.1021/JAFCAU.2011.59.ISSUE-13;PAGE:STRING:ARTICLE/CHAPTER.

Oliveira, R. V. M., Santos, A. F., Santos, M. D. L., da Cunha, G. C., & Romão, L. P. C. (2022). Magnetic solid-phase extraction of bisphenol A from water samples using nanostructured material based on graphene with few layers and cobalt ferrite. *Microchemical Journal, 181*, Article 107741. https://doi.org/10.1016/J.MICROC.2022.107741

OuYang, Y., Wang, Q., Lou, Y., Song, X., & Wu, M. (2025). Smart antibacterial packaging films prepared by TOCNC/CS nanoparticles stabilized Pickering emulsion to prolong shelf-life of fresh pork. *Innovative Food Science & Emerging Technologies, 106*, Article 104317. https://doi.org/10.1016/J.IFSET.2025.104317

Palanisamy, Y., Kadirvel, V., & Ganesan, N. D. (2025). Recent technological advances in food packaging: Sensors, automation, and application. *Sustainable Food Technology, 3*(1), 161–180. https://doi.org/10.1039/D4FB00296B

Pallach, R., Keupp, J., Terlinden, K., Frentzel-Beyme, L., Kloß, M., Machalica, A., … Henke, S. (2021). Frustrated flexibility in metal-organic frameworks. *Nature Communications, 12*(1), 4097. https://doi.org/10.1038/S41467-021-24188-4

Peñalver, R., Arroyo-Manzanares, N., Campillo, N., & Viñas, P. (2021). Targeted and untargeted gas chromatography-mass spectrometry analysis of honey samples for determination of migrants from plastic packages. *Food Chemistry, 334*, Article 127547. https://doi.org/10.1016/J.FOODCHEM.2020.127547

Pezhhanfar, S., Farajzadeh, M. A., Hosseini-Yazdi, S. A., & Afshar Mogaddam, M. R. (2022a). Analytical application of MIL-53 (Al) for the extraction of pesticides from fruit juices following their preconcentration through dispersive liquid-liquid microextraction. *Talanta Open, 5*, Article 100121. https://doi.org/10.1016/J.TALO.2022.100121

Pezhhanfar, S., Farajzadeh, M. A., Hosseini-Yazdi, S. A., & Afshar Mogaddam, M. R. (2022b). Analytical application of MIL-53 (Al) for the extraction of pesticides from fruit juices following their preconcentration through dispersive liquid-liquid microextraction. *Talanta Open, 5*, Article 100121. https://doi.org/10.1016/J.TALO.2022.100121

Pezhhanfar, S., Farajzadeh, M. A., Hosseini-Yazdi, S. A., & Afshar Mogaddam, M. R. (2022c). Analytical application of MIL-53 (Al) for the extraction of pesticides from fruit juices following their preconcentration through dispersive liquid-liquid microextraction. *Talanta Open, 5*, Article 100121. https://doi.org/10.1016/J.TALO.2022.100121

Quan, X., Sun, Z., Xu, J., Liu, S., Han, Y., Xu, Y., … Zhang, X. (2020). Construction of an aminated MIL-53(Al)-functionalized carbon nanotube for the efficient removal of bisphenol AF and metribuzin. *Inorganic Chemistry, 59*(5), 2667–2679. https://doi.org/10.1021/ACS.INORGCHEM.9B02841

Regueiro, J., Breidbach, A., & Wenzl, T. (2015). Derivatization of bisphenol A and its analogues with pyridine-3-sulfonyl chloride: Multivariate optimization and fragmentation patterns by liquid chromatography/orbitrap mass spectrometry. *Rapid Communications in Mass Spectrometry, 29*(16), 1473–1484. https://doi.org/10.1002/RCM.7242

Rehman, T. U., Agnello, S., Gelardi, F. M., Calvino, M. M., Lazzara, G., Buscarino, G., & Cannas, M. (2025). Exploring Fe3+ cation exchange dynamics in fluorescent MIL-53 (Al) MOF: Solid-state photoluminescence and structural insights. *Materials Chemistry and Physics, 332*, Article 130237. https://doi.org/10.1016/J.MATCHEMPHYS.2024.130237

Schecter, A., Malik, N., Haffner, D., Smith, S., Harris, T. R., Paepke, O., & Birnbaum, L. (2010). Bisphenol A (BPA) in U.S. food. *Environmental Science and Technology, 44*(24), 9425–9430. https://doi.org/10.1021/ES102785D

Shao, P., Liu, L., Yu, J., Lin, Y., Gao, H., Chen, H., & Sun, P. (2021). An overview of intelligent freshness indicator packaging for food quality and safety monitoring. *Trends in Food Science & Technology, 118*, 285–296. https://doi.org/10.1016/J.TIFS.2021.10.012

Silva Maciel, L., Hříbková, M., & Herodes, K. (2024). Evaluation of in-house-built pipette-tip micro-solid-phase extraction devices for sample preparation in the analysis of amino compounds by liquid chromatography-tandem mass spectrometry. *Journal of Chromatography A, 1738*, Article 465480. https://doi.org/10.1016/J.CHROMA.2024.465480

Skans, I., Dyosiba, X. L., Mnguni, M., & Nomngongo, P. N. (2025a). MIL-53(Al)-MOF sorbents in dispersive micro-solid phase extraction of penicillins from water. *Talanta Open, 11*, Article 100460. https://doi.org/10.1016/J.TALO.2025.100460

Skans, I., Dyosiba, X. L., Mnguni, M., & Nomngongo, P. N. (2025b). MIL-53(Al)-MOF sorbents in dispersive micro-solid phase extraction of penicillins from water. *Talanta Open, 11*, Article 100460. https://doi.org/10.1016/J.TALO.2025.100460

Skans, I., Dyosiba, X. L., Mnguni, M., & Nomngongo, P. N. (2025c). MIL-53(Al)-MOF sorbents in dispersive micro-solid phase extraction of penicillins from water. *Talanta Open, 11*, Article 100460. https://doi.org/10.1016/J.TALO.2025.100460

Song, J., Qian, H. L., Xu, S. T., Yang, C., & Yan, X. P. (2025). Boronate affinity molecularly imprinted covalent organic framework for highly selective recognition and extraction of zearalenone. *Food Chemistry, 486*, Article 144590. https://doi.org/10.1016/J.FOODCHEM.2025.144590

Valenzuela, I. E., Valencia, S., Muñoz-Acevedo, J. C., Paim, A. P. S., & Pabón-Gelves, E. (2025). Adsorptive removal of losartan, bisphenol A, and triclosan in aqueous solutions using a graphene oxide-enhanced MOF-Zn composite. *Environmental Science and Pollution Research, 32*(45), 25992–26015. https://doi.org/10.1007/S11356-025-36961-9

Vállez-Gomis, V., Benedé, J. L., Lara-Molina, E., López-Nogueroles, M., & Chisvert, A. (2024). A miniaturized stir bar sorptive dispersive microextraction method for the determination of bisphenols in follicular fluid using a magnetic covalent organic framework. *Analytica Chimica Acta, 1289*, Article 342215. https://doi.org/10.1016/J.ACA.2024.342215

Vandenberg, L. N., Colborn, T., Hayes, T. B., Heindel, J. J., Jacobs, D. R., Lee, D. H., … Myers, J. P. (2012). Hormones and endocrine-disrupting chemicals: Low-dose effects and nonmonotonic dose responses. *Endocrine Reviews, 33*(3), 378–455. https://doi.org/10.1210/ER.2011-1050

Vennapusa, J. R., Singh, J., & Chattopadhyay, S. (2022). Curding of milk in incubator utilizing latent heat of lauric acid in winter. *Energy Storage, 4*(3), Article e307. https://doi.org/10.1002/EST2.307

Wang, Q., Chen, L., Cui, X., Zhang, J., Wang, Y., & Yang, X. (2023). Determination of trace bisphenols in milk based on Fe3O4@NH2-MIL-88(Fe)@TpPa magnetic solid-phase extraction coupled with HPLC. *Talanta, 256*, Article 124268. https://doi.org/10.1016/J.TALANTA.2023.124268

Wang, Q., Zheng, Y., Deng, B., Chen, D., Jia, L., & Shi, N. (2024). Automated kapok fiber-based pipette-tip solid-phase extraction coupled with liquid chromatography-tandem mass spectrometry for rapid and sensitive analysis of tyrosine kinase inhibitors in plasma. *Journal of Chromatography A, 1736*, Article 465420. https://doi.org/10.1016/J.CHROMA.2024.465420

Xiang, J., Zhou, P., Mei, H., Liu, X., Wang, H., Wang, X., & Li, Y. (2023). Highly efficient nanocomposites based on molecularly imprinted magnetic covalent organic frameworks for selective extraction of bisphenol A from liquid matrices. *Microchimica Acta, 190*(5), 1–15. https://doi.org/10.1007/S00604-023-05778-Z/METRICS

Zahmatkesh Anbarani, M., & Bonyadi, Z. (2025). Review on the utilization of metal organic frameworks for eliminating bisphenols from aqueous solutions: Mechanisms and performance insights. *Chemical Engineering Journal Advances, 24*, Article 100920. https://doi.org/10.1016/J.CEJA.2025.100920

Zhang, G., Wo, R., Sun, Z., Hao, G., Liu, G., Zhang, Y., … Jiang, W. (2021). Effective magnetic mofs adsorbent for the removal of bisphenol a, tetracycline, Congo red and methylene blue pollutions. *Nanomaterials, 11*(8), 1917. https://doi.org/10.3390/NANO11081917/S1

Zhang, G., Wo, R., Sun, Z., Xiao, L., Liu, G., Hao, G., … Jiang, W. (2021). Amido-functionalized magnetic metal−organic frameworks adsorbent for the removal of bisphenol A and tetracycline. *Frontiers in Chemistry, 9*, Article 707559. https://doi.org/10.3389/FCHEM.2021.707559/FULL

Zhang, N., Li, Y., Liu, M., Hu, M., Wang, H., Ma, W., & Lu, M. (2025). Facile synthesis of fluorine-functionalized long-chain metal–organic frameworks for highly efficient enrichment and sensitive detection of bisphenols in water samples. *Journal of Hazardous Materials, 493*, Article 138382. https://doi.org/10.1016/J.JHAZMAT.2025.138382

Zhou, M., Wu, Y., Nan Qiao, J., Zhang, J., McDonald, A., Li, G., & Li, F. (2013). The removal of bisphenol A from aqueous solutions by MIL-53(Al) and mesostructured MIL-53(Al). *Journal of Colloid and Interface Science, 405*, 157–163. https://doi.org/10.1016/J.JCIS.2013.05.024

Zhu, S., Lou, X., Zhu, J., Song, Z., Hao, Y., Yang, J., & Lu, M. (2024). Ultra-stable Co3O4/NiCo2O4 double-shelled hollow nanocages as headspace solid-phase microextraction coating for enhanced capture of polychlorinated biphenyls. *Chemical Engineering Journal, 488*, Article 150876. https://doi.org/10.1016/J.CEJ.2024.150876